Supplemental Information

Kappa Opioid Receptor Distribution and Function in Primary Afferents

Lindsey M. Snyder, Michael C. Chiang, Emanuel Loeza-Alcocer, Yu Omori, Junichi Hachisuka, Tayler D. Sheahan, Jenna R. Gale, Peter C. Adelman, Elizabeth I. Sypek, Stephanie A. Fulton, Robert L. Friedman, Margaret C. Wright, Melissa Giraldo Duque, Yeon Sun Lee, Zeyu Hu, Huizhen Huang, Xiaoyun Cai, Kimberly A. Meerschaert, Vidhya Nagarajan, Toshiro Hirai, Gregory Scherrer, Daniel H. Kaplan, Frank Porreca, Brian M. Davis, Michael S. Gold, H. Richard Koerber, and Sarah E. Ross

Supplemental Data

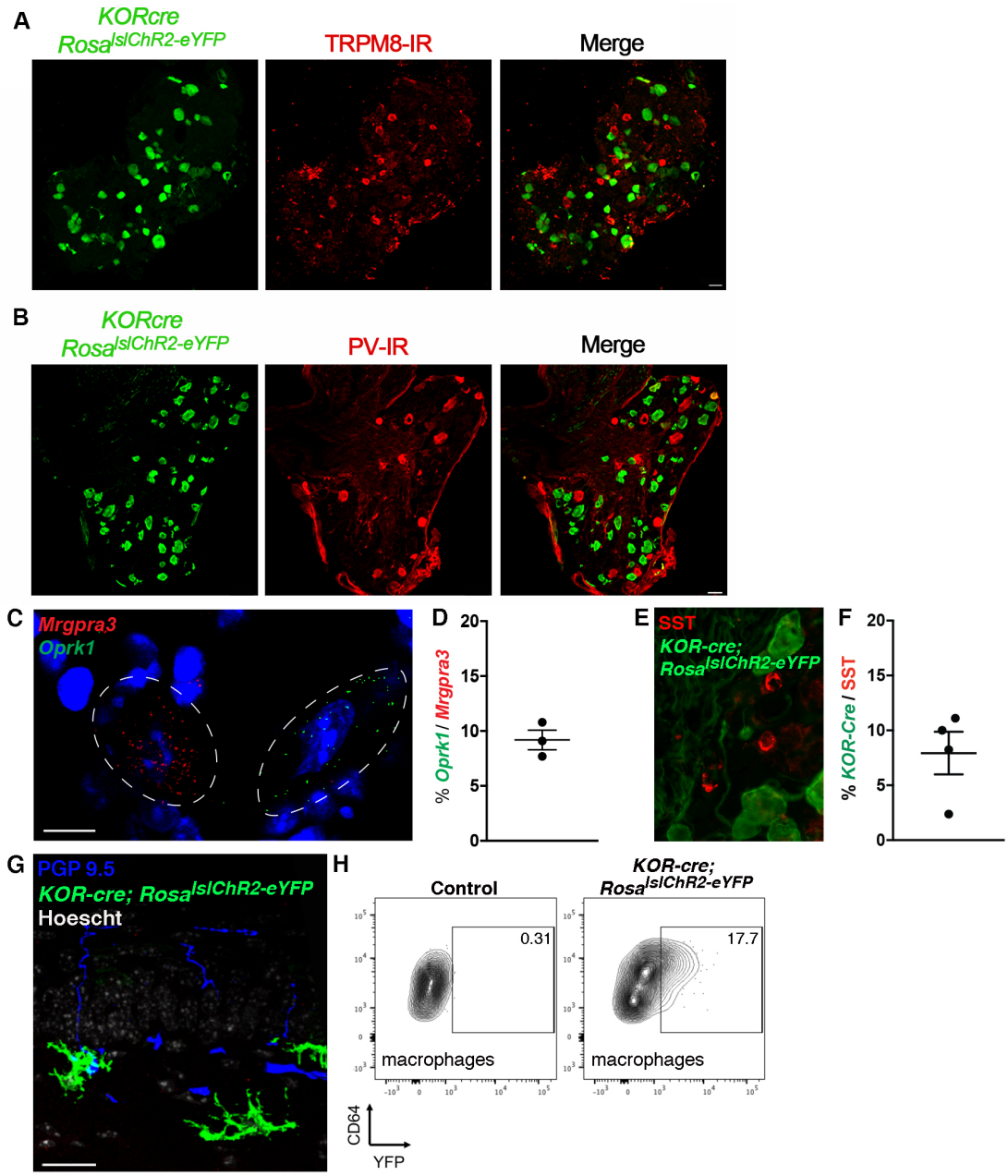

Figure S1. related to Figure 2. Characterization of *KOR-cre* and *Oprk1* expression.

A - B. Immunohistochemistry of lumbar DRG sections showing little to no overlap between *KOR-cre; Rosa*$^{lslChR2\text{-}eYFP}$ positive neurons and TRPM8-IR (A) or parvalbumin (PV-IR; B), indicating that *KOR-cre* neurons do not include putative cool-sensing neurons or putative proprioceptors, respectively.

C – D. Representative image (C) and quantification (D) of double in situ hybridization of lumbar DRG sections showing little overlap between *Oprk1 and MrgprA3.* Data are mean +/- SEM (n = 3 mice). Scale bar = 10 μm.

E – F. Representative image (E) and quantification (F) immunohistochemistry of lumbar DRG sections showing little overlap between somatostatin (SST) and *KOR-cre; Rosa*$^{lslChR2\text{-}eYFP}$*.* Data are mean +/- SEM (n = 4 mice).

G. Immunohistochemistry of the skin *KOR-cre; Rosa*$^{lslChR2\text{-}eYFP}$ mouse showing recombination in cells in the dermis.

H. Flow cytometry of skin from *KOR-cre; Rosa*$^{lslChR2\text{-}eYFP}$ mice or a genetic control reveals GFP expression in macrophages. In experiments looking at primary afferent terminals in the skin, we noted the recombination of some dermal cells (H) that turned out to be macrophages upon examination by flow cytometry (H). However, we were unable to detect *Oprk1* mRNA in these cells, either by RT-PCR or in situ hybridization, possibly due to a very low abundance or transient expression of *Oprk1* in these cells.

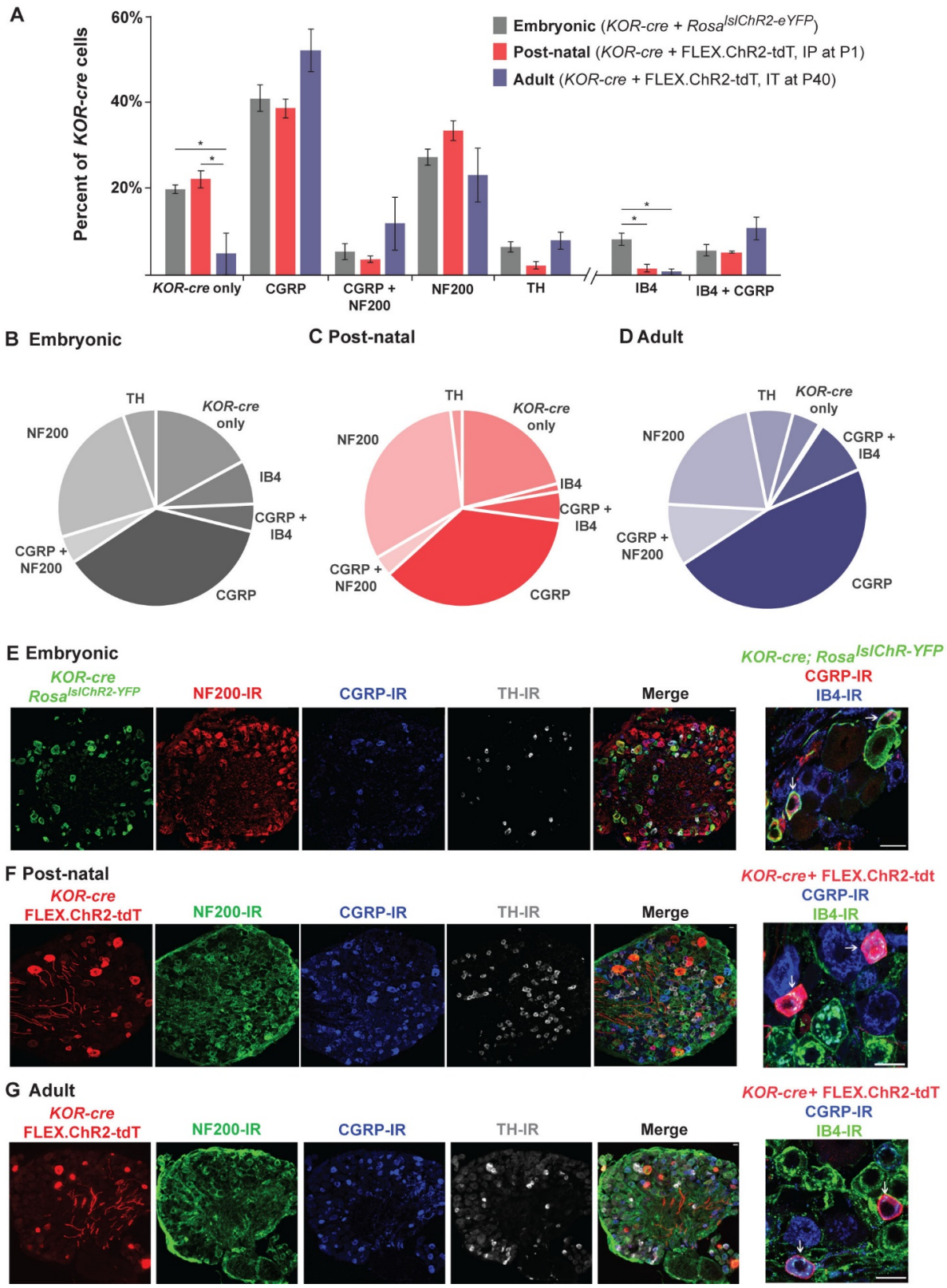

Figure S2. Related to Figure 2. Comparison of *KOR-cre* mediated recombination at different times during development. Figure legend continued on next page

Figure S2, continued.

A. To determine whether *KOR-cre* mediated recombination varies across an animal lifespan, the recombination that was observed following the introduction of a Cre-dependent reporter at three different stages of development was compared. *KOR-cre* mice were either crossed with Ai9 mice (*Rosa*$^{lslChR2\text{-}eYFP}$), or infected with Cre-dependent virus at either P1 or in adult mice. Sections from DRG were quadruple labeled with the reporter and antibodies against NF200, CGRP, and TH, and the percentage of genetically-labeled cells that co-localize with one or more of these three markers was quantified. Gray bars represent the *KOR-cre* positive population in *KOR-cre Rosa*$^{lslChR2\text{-}eYFP}$ mice, red bars represent the *KOR-cre* positive population in mice injected with FLEX.ChR2-tdT virus IP at P1, and blue bars represent the *KOR-cre* positive population in mice injected with FLEX.ChR2-tdT virus IT at P40. When infection occurs in adult, only 5% of labeled *KOR-cre* afferents do not co-localize with either CGRP, NF200 or TH (i.e., *KOR-cre* only). However, if the reporter is introduced during embryonic or early post-natal development, the fraction of *KOR-cre* only afferents is significantly increased (One-way ANOVA with Tukey's multiple comparison's test, *, $p < 0.05$, n = 3 mice). In a separate experiment, sections were co-stained with antibodies to CGRP and with IB4. For each condition, *KOR-cre* neurons that co-localized with both CGRP and IB4 were observed. However, when the reporter was introduced embryonically, *KOR-cre* neurons that co-localized with IB4 but not CGRP (i.e., IB4 only) were observed. In contrast, when the reporter was introduced later, a significant decrease in the proportion of *KOR-cre* afferents that co-stain with IB4 only was observed (One-way ANOVA with Tukey's multiple comparison's test, *, $p < 0.05$, n = 3 mice). Together, these findings suggest that labeling with the *KOR-cre* allele becomes more restricted over the course of development. Data are presented at mean ± SEM. Similar results were seen whether Cre-dependent viruses were introduced via intrathecal or intrasciatic injection in adult mice (n = 3 mice per viral delivery route, data not shown).

B - D. Pie charts representing the proportion of *KOR-cre* neurons that co-localize with various neurochemical markers. Charts illustrate that the proportion of each group remains similar across *KOR-cre Rosa*$^{lslChR2\text{-}eYFP}$ mice, *KOR-cre* + FLEX.ChR2-tdT delivered IP at P1 mice, and *KOR-cre* + FLEX.ChR2-tdT delivered IT at P40 mice.

E - G. Representative image of a lumbar DRG section showing co-localization of *KOR-cre* neurons with NF200, CGRP, TH, and IB4 in *KOR-cre Rosa*$^{lslChR2\text{-}eYFP}$ mice (E), *KOR-cre* + FLEX.ChR2-tdT delivered IP at P1 mice (F), and *KOR-cre* + FLEX.ChR2-tdT delivered IT at P40 mice (G). Arrows indicate *KOR-cre* positive neurons that co-localize with both CGRP and IB4.

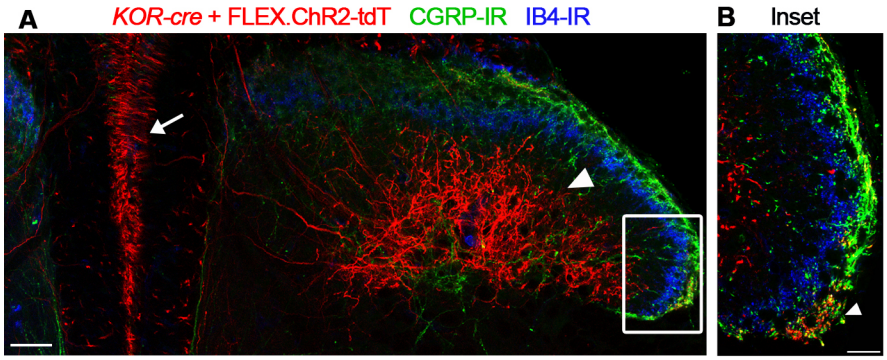

Figure S3. Related to Figure 3. *KOR-cre* labeled afferents include putative LTMRs that target the dorsal columns

A - B. Representative image of *KOR-cre* primary afferent terminals in the lumbar spinal cord. *KOR-cre* neurons were infected via an IP injection of AAV.FLEX.ChR2-tdT at P1. Arrowhead indicates *KOR-cre* positive terminals in the deeper dorsal horn below the IB4 band (A) and in the superficial dorsal horn that overlap with the CGRP-IR band (B). Arrow indicates *KOR-cre* positive fibers that appear to ascend in the dorsal column pathway. A similar pattern was observed in n = 3 mice.

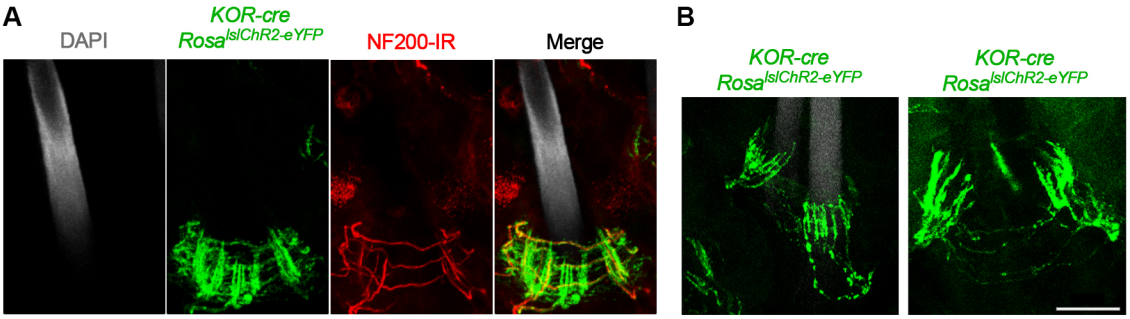

Figure S4. Related to Figure 3. *KOR-cre* labeled afferents form circumferential and lanceolate endings that target multiple hair types

A - B. Wholemount IHC of the thoracic skin from a *KOR-cre* *Rosa*$^{lslChR2\text{-}eYFP}$ mouse co-stained showing *KOR-cre* positive lanceolate (left), and lanceolate and circumferential endings (right) innervating hair follicles in the back skin of a guard hair (A) and zigzag and/or awl/auchene hairs (B).

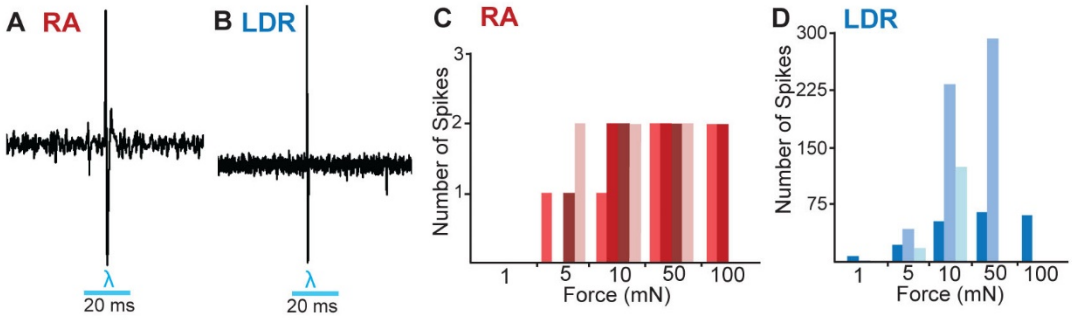

E

			Number of Spikes					
Type	CV	Threshold	1mN	5mN	10mN	25mN	50mN	100mN
RA	5.63	5	0	1	1	2	2	
RA	13.89	10		0	2	2	2	
RA	6.64	5	0	1	2	2		
RA	4.61	5	0	2	2	2		
LDR	13.28	5	0	7	22	53	65	63
LDR	6.67	5	0	1	43	233	294	
LDR	8.81	5		1	*	*	*	*
LDR	7.03	10		0	18	125		

*There is a second cell present in the recording and making accurate spike counting difficult.

Figure S5. Related to Figure 3. Electrophysiological characteristics of myelinated *KOR-cre* afferents

Teased-fiber recordings were performed in a skin-nerve preparation of the dorsal hindpaw from *KOR-cre; Rosa*$^{lslChR2\text{-}eYFP}$ *mice.*

A - B. Optogenetic tagging was performed to identify *KOR-cre* afferents. Example traces of responses to blue light stimulation (470 nm, 20 ms) of the receptive field of afferents that were subsequently characterized as rapidly adapting (RA, A) or as large dynamic range (LDR; B).

C - D. Graph of the number of spikes observed following mechanical stimulation of the receptive field with a piezo-electric stimulator at varying forces. Each shade represents an individual cell's response across stimulus intensities. Rapidly adapting afferents fired only 1 or 2 spikes, irrespective of the force (C); large dynamic range fibers showed an increase in the spike number as a function of force.

E. Table displaying the measured conduction velocity (CV), mechanical threshold, and the number of spikes following a given stimulus for each *KOR-cre* neuron recorded.

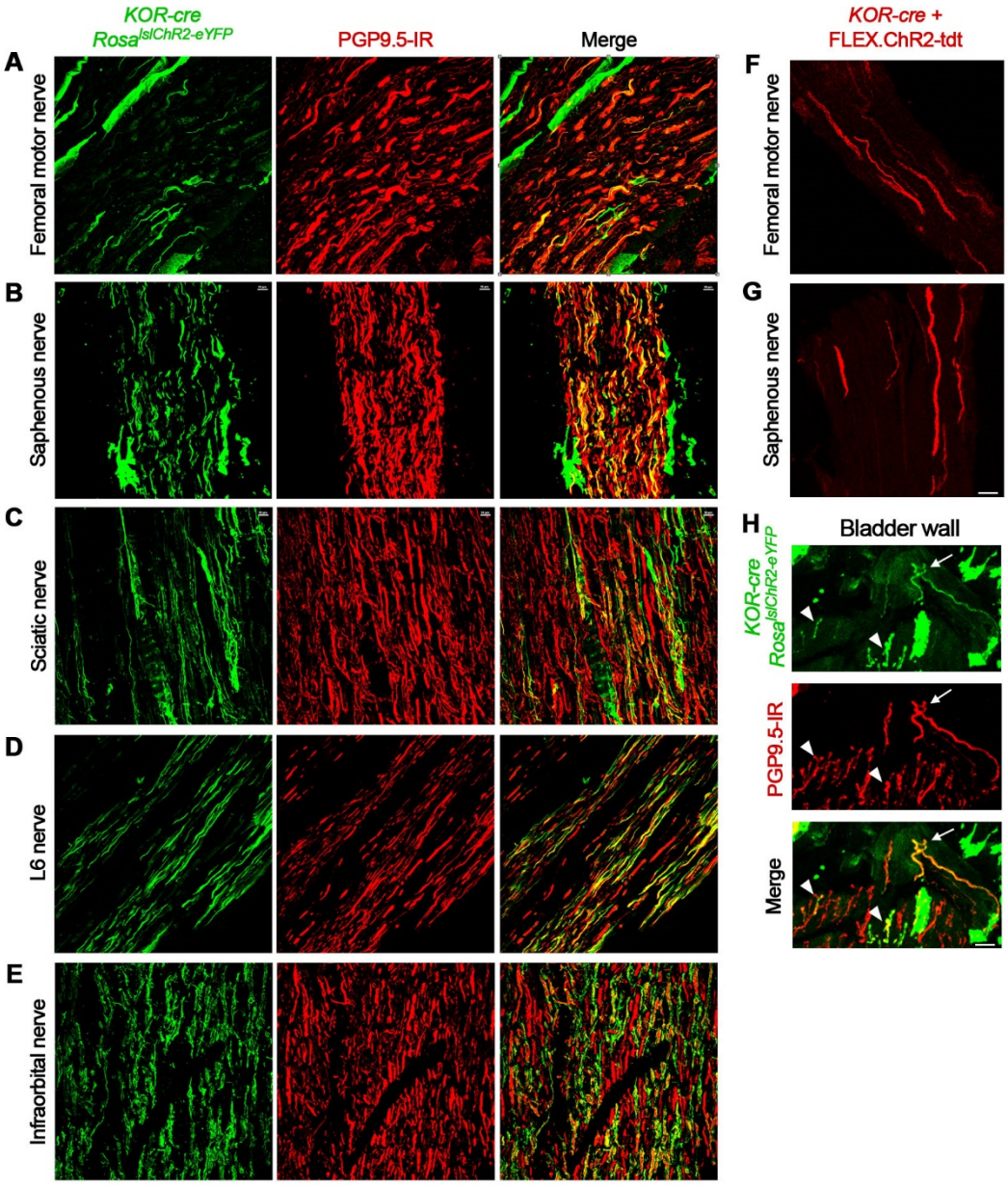

Figure S6. Related to Figure 4. *KOR-cre* afferents target tissues throughout the body

A – E. Representative images of IHC from *KOR-cre Rosa*$^{lslChR2\text{-}eYFP}$ mice showing *KOR-cre* positive fibers that co-localize with PGP9.5-IR in the femoral motor nerve, (A) saphenous nerve (B), sciatic nerve (C), L6 nerve (D) and the infraorbital nerve (E). These data suggest that KOR-expressing neurons innervate multiple tissue types throughout the body.

F – G. Representative images of IHC from *KOR-cre* + FLEX.ChR2-tdt delivered IT at P40 mice in the femoral motor nerve (F) and the saphenous nerve (G) that is consistent with the pattern observed in *KOR-cre; Rosa*$^{lslChR2\text{-}eYFP}$ mice.

H. Representative images of IHC from *KOR-cre Rosa*$^{lslChR2\text{-}eYFP}$ mice showing *KOR-cre* positive fibers that co-localize with PGP9.5-IR in the bladder wall that terminate in both the lamina propria (arrows) and the muscularis (arrowheads).

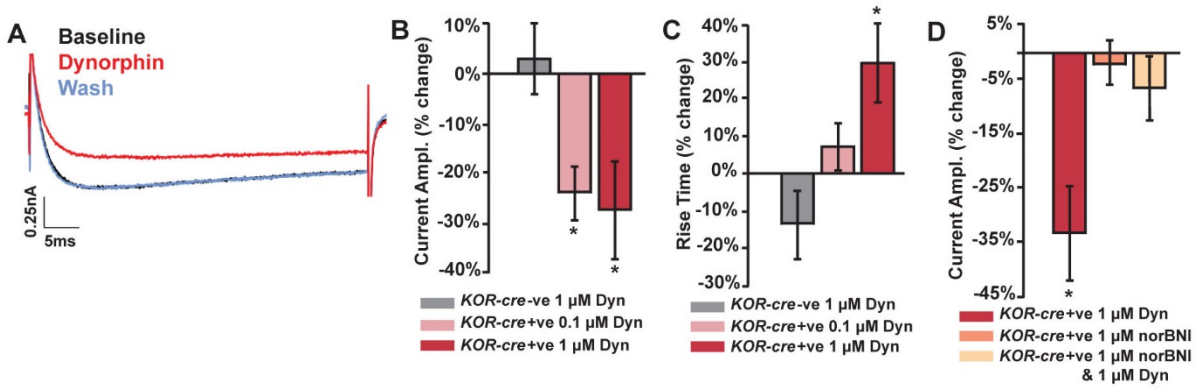

Figure S7. Related to Figure 5. The inhibition of VGCC by dynorphin is blocked by the opioid receptor antagonist norBNI.

A. Representative traces of VGCC in a *KOR-cre*-positive neuron at baseline (black), in the presence of dynorphin (1 µm; red), and after washout (blue). Neurons were held at -70 mV and a 50 ms step to 0 mV was applied.

B - C. Quantification of the percent change in current amplitude (B) or rise time (C) of either *KOR-cre* negative neurons (gray; n = 5 neurons), *KOR-cre* positive neurons in the presence of 0.1 µm dynorphin (pink; n = 7 neurons), or of *KOR-cre* positive neurons in the presence of 1 µm dynorphin (red; n = 6 neurons). There was a significant decrease in current amplitude in the presence of either 0.1 or 1 µm dynorphin in *KOR-cre* positive neurons relative to baseline (*, paired t-test, $p < 0.05$). There was a significant increase in the rise time in the presence of 1 µm dynorphin in *KOR-cre* positive neurons relative to baseline (*, paired t-test, $p < 0.05$). Data are presented as mean ± SEM.

D. Quantification of the percent change in current amplitude of either *KOR-cre* positive neurons in the presence of dynorphin (1 µm; red), in the presence of norBNI (1 µm; orange), or in the presence of dynorphin (1 µm) and norBNI (1 µm; light orange). n = 3 neurons. Only dynorphin alone caused a significant decrease in the current amplitude (*, paired t-test, $p < 0.05$). Data are presented as mean ± SEM.

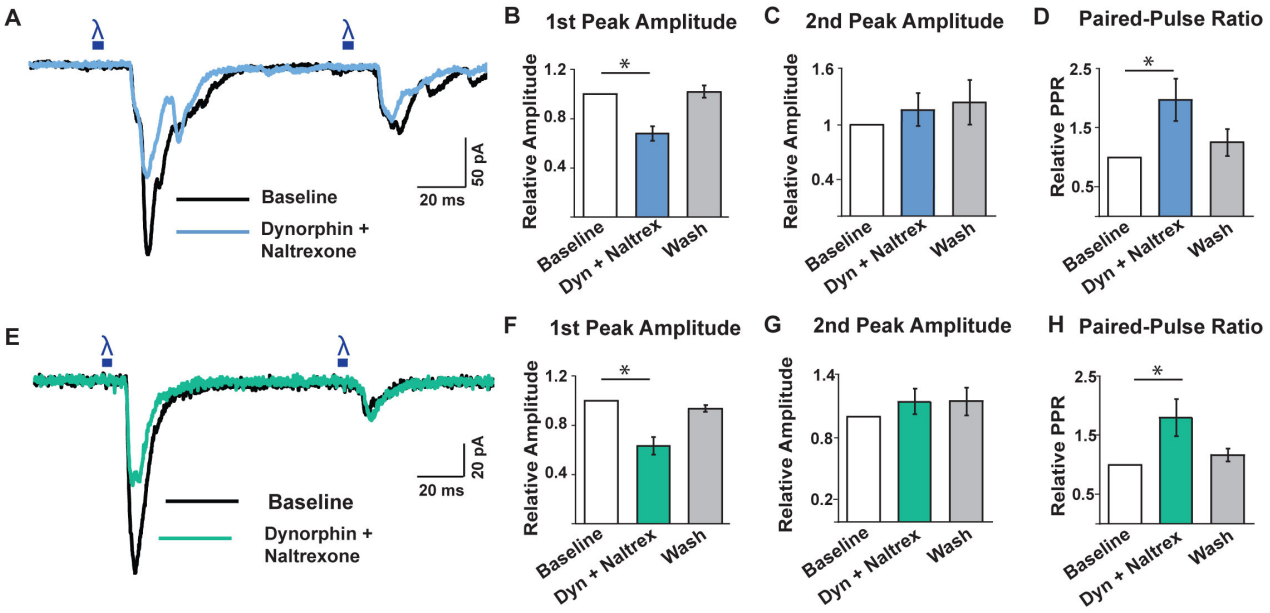

Figure S8. Related to Figure 6. Dynorphin-mediated inhibition of glutamate release from KOR-expressing afferents is not inhibited by nalterone.

A. Representative trace of whole-cell patch clamp recording from a lamina I neuron at baseline (black) and during bath application of dynorphin (1 μm) + naltrexone (1 μm) (blue). Two 5 ms pulses of blue light were given 100 ms apart to elicit light-evoked EPSCs.

B - D. Quantification of the 1st eEPSC relative amplitude, 2nd eEPSC relative amplitude, and relative paired pulse ratio during baseline (white), drug (blue), and wash (gray) conditions in recordings from lamina I dorsal horn neurons following blue light stimulation of *KOR-cre* positive primary afferent terminals in *KOR-cre* + FLEX.ChR2 IP at P1. There was a significant decrease in 1st peak amplitude during dynorphin + naltrexone application compared to baseline in lamina I neurons (B). There was no significant change in 2nd peak amplitude during dynorphin + naltrexone application compared to baseline in lamina I neurons (C). There was a significant increase in the paired pulse ratio during dynorphin + naltrexone application compared to baseline in lamina I neurons (D). Data are presented as mean ± SEM. * $p < 0.05$, one-way ANOVA followed by Dunnett's multiple comparison's test, n = 15 cells.

E. Representative trace of whole-cell patch clamp recording from a lamina III neuron at baseline (black) and during bath application of dynorphin (1 μm) + naltrexone (1 μm) (green). Two 5 ms pulses of blue light were given 100 ms apart to elicit light-evoked EPSCs.

F - H. Quantification of the 1st eEPSC relative amplitude, 2nd eEPSC relative amplitude, and relative paired pulse ratio during baseline (white), drug (green), and wash (gray) conditions in recordings from lamina III dorsal horn neurons following blue light stimulation of the dorsal root in *KOR-cre* $Rosa^{lslChR2\text{-}eYFP}$ mice. There was a significant decrease in 1st peak amplitude during dynorphin + naltrexone application compared to baseline in lamina III neurons (F). There was no significant change in 2nd peak amplitude during dynorphin + naltrexone application compared to baseline in lamina III neurons (G). There was a significant increase in the paired pulse ratio during dynorphin + naltrexone application compared to baseline in lamina III neurons (G) Data are presented as mean ± SEM. * $p < 0.05$, one-way ANOVA followed by Dunnett's multiple comparison's test, n = 6 cells.

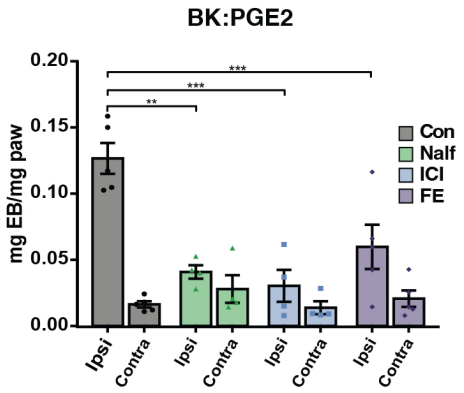

Figure S9. Related to Figure 7. KOR agonists inhibit neurogenic inflammation induced by bradykinin and prostaglandin E2

Evans blue extravasation upon injection of bradykinin:prostaglandin E2 (10 μM:10 μM, 10μL) into the ipsilateral paw of mice pretreated with vehicle (Con), nalfurafine (Nalf, 20 μg/kg), ICI204,448 (ICI, 10 mg/kg), or FE200665 (FE, 12 mg/kg), as indicated. Data are mean ± SEM and symbols represent data points from individual animals (two-way ANOVA followed by Tukey's post hoc test; ** $p < 0.01$; *** $p < 0.001$, n = 4 – 5 mice/condition).

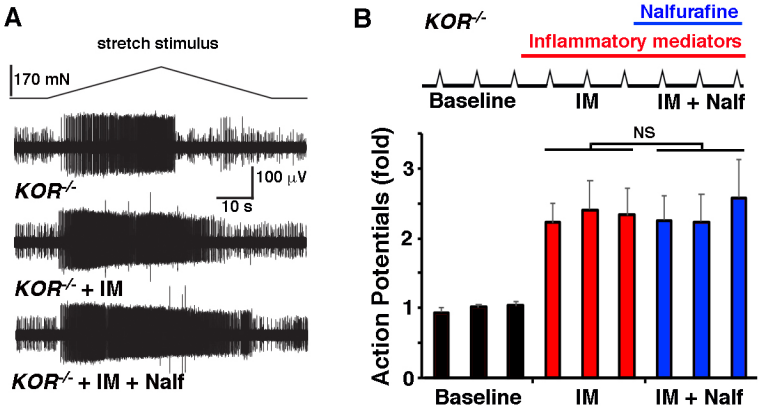

Figure S10. Related to Figure 7. The effects of nalfurafine on the inhibition of sensitization are specific to KOR.

A. - B. Mice lacking *KOR* show no response to nalfurafine. Typical recording (A) and quantification (B) of a teased fiber response in a *KOR-/-* mouse to stretch (top trace) before (baseline) and after application of inflammatory mediators (IM: histamine, bradykinin, prostaglandin E2, and serotonin, each at 10 μM) or the combination of inflammatory mediators and 10 nM nalfurafine (IM + Nalf). Data represent mean (normalized to the average baseline response) + SEM (One-way RM AVOVA, followed by Holm-Sidak post hoc; NS > 0.05; n = 6 afferents

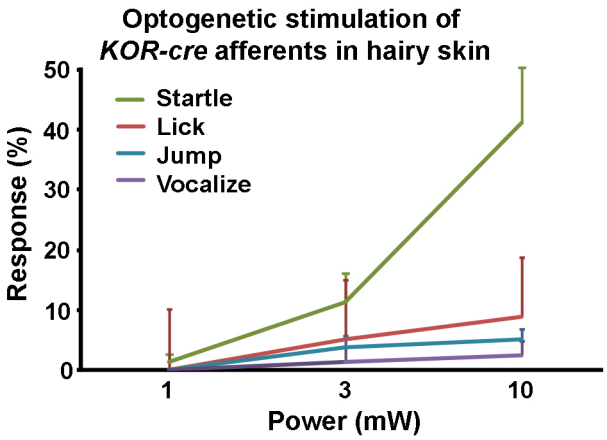

Figure S11. Related to Figure 8. Optogenetic activation of *KOR-cre* afferents that innervate hairy skin elicits primarily a startle response, accompanied by occasional licking, jumping or vocalization

Blue light (470 nm) LED stimulation (1 s) was applied to shaved abdomen skin of *KOR-cre; Rosa*$^{lslChR2\text{-}eYFP}$ and the frequency of response (startle, site-directed licking, jumping or vocalization) was quantified at three different LED intensities (1 mW, 3 mW, and 10 mW). Data are presented as mean ± SEM (n = 8 mice/group with 10 stimulus presentations per mouse).

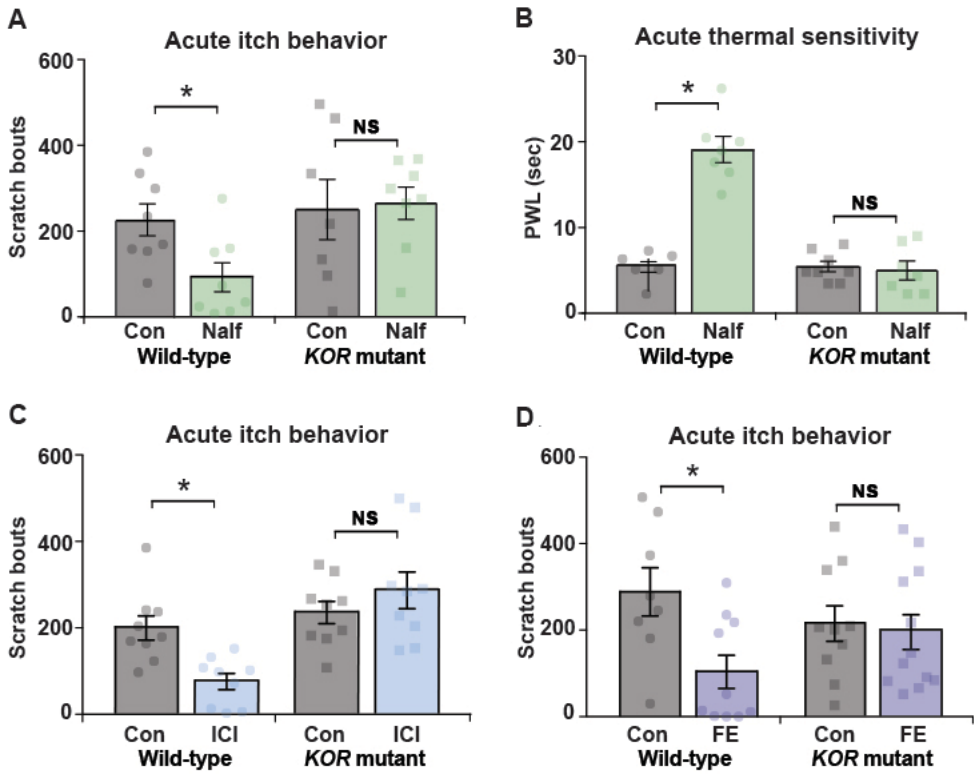

Figure S12. Related to Figure 8.n The effects of nalfurafine, ICI204,488 and FE200665 on itch and pain behaviors are specific to KOR

Nalfurafine (Nalf, 200 µg/kg), ICI204,488 (ICI, 10 mg/kg), or FE200665 (FE, 12 mg/kg) were given IP 15 minutes prior to the start of the behavioral assays. *KOR* mutant mice, which are homozygous for the *KOR-cre* allele, and their wild-type littermates were used for these experiments. All data are presented as mean ± SEM and colored shapes represent data points from individual mice.

A. Nalfurafine significantly decreased chloroquine-induced scratching behavior (20 µl intradermal, 200 µg) in wild-type mice (*, $p < 0.05$, two-way ANOVA with General Linear Hypothesis Test). In *KOR* mutant mice, nalfurafine had no significant effect (NS, $p > 0.05$). n = 7 – 8 mice/group.

B. Nalfurafine significantly paw withdrawal latency to thermal heat (Hargreaves' test) in wild-type mice, (*, $p < 0.001$, two-way ANOVA with General Linear Hypothesis Test). In *KOR* mutant mice, nalfurafine had no significant effect (NS, $p > 0.05$). n = 7 – 8 mice/group.

C. ICI204,448 significantly decreased chloroquine-induced scratching behavior (20 µl intradermal, 200 µg) in wild-type mice (*, $p < 0.001$, two-way ANOVA with General Linear Hypothesis Test,). In *KOR* mutant mice, ICI204,448 had no significant effect (NS, $p > 0.05$). n = 9 mice/group.

D. FE200665 significantly decreased chloroquine-induced scratching behavior (20 µl intradermal, 200 µg) in wild-type mice, but not in *KOR* mutant mice (*, $p < 0.01$, two-way ANOVA with General Linear Hypothesis Test,). In *KOR* mutant mice, ICI204,448 had no significant effect (NS, $p > 0.05$). n = 8 – 12 mice/group.